Contents

List of Variables

$AR = aspect\ ratio$
$\alpha = geometric\ angle\ of\ attack$
$a_0 = lift\ curve\ slope$
$\alpha_{eff} = effective\ angle\ of\ attack$
$\alpha_i = induced\ angle\ of\ attack$
$\alpha_{L=0} = zero\ lift\ angle\ of\ attack$
$b = wingspan$
$\lambda = taper\ ratio$
$rc = root\ chord$
$tc = tip\ chord$
$c = chord\ length$
$w = downwash\ velocity$
$D_i = induced\ drag$
$D_i' = induced\ drag\ per\ unit\ span$
$L' = lift\ per\ unit\ span$
$L = lift$
$\rho_\infty = free\ stream\ density$
$V_\infty = free\ stream\ velocity$
$V_{eff} = net\ effective\ free\ stream\ velocity$
$w = downwash\ velocity$
$\Gamma = circulation$

List of Tables

List of Figures

Abstract

This paper utilizes a numerical implementation of Prandtl's classical lifting line theory to predict stall characteristics of finite wings with a NACA 0015 and a NACA 4418 airfoil section. The numerical implementation was able to predict lift coefficients from the spanwise circulation distribution within 10% accuracy for most of the data, with much higher accuracy in certain regions. The program written in MATLAB® was used to observe the effects of aerodynamic coefficients from cambering the airfoil, varying the Reynolds number, and varying the aspect ratio. Cambering the airfoil provides more lift and leads to a less precipitous drop in lift at stall than a symmetric airfoil. Low aspect ratio wings experience more downwash leading to a decrease in lift and increase in induced drag. Increasing the Reynolds number corresponds to a reduction in the maximum lift coefficient. At extreme angles of attack, the effect of varying Reynolds number has little to no significance on the lift coefficients.

1 - Introduction

The introduction of the circulation theory of lift described by the Kutta-Joukowski theorem allowed Ludwig Prandtl to formulate the first practical aerodynamic theory for wings of finite span. In the period between 1911-1918, Prandtl and colleagues in Göttingen Germany, were able to justify that aerodynamic properties of finite wings could be understood by first studying airfoils, and then correcting the aerodynamic definitions to accurately represent the finite wing. Coming up with a mathematical representation of this correction was the main objective behind the creation of Prandtl's classical lifting line theory. Lifting line theory revolutionized aircraft at the time and is still used today for preliminary calculations, as well as understanding the aerodynamic properties for wings of different geometry (Anderson, 2016, pp. 427-430).

Since then, the advancements of high-speed computers and numerical methods has pushed the computational limits of aerodynamic theory in the past few decades. The development of public and proprietary software has enabled a more thorough understanding of flight theory and has contributed to more efficient high-performance aircraft. For subsonic aerodynamics, preliminary calculations for finite wing properties can still be done today using Prandtl's lifting line theory. There are many methods that reach far beyond the scope of Prandtl's classical theory to correct for compressibility, sweep, 3D

flow effects and drag, however, these methods are more computationally expensive which is why original lifting line theory is still useful.

Unlike classical lifting line theory, a numerical implementation is useful for reasonably predicting stall at the critical angle of attack and predicting the lift coefficients of the linear and nonlinear regions of the lift coefficient curve. The usefulness of this implementation is that the aerodynamic properties of different finite wings with different geometric properties can be estimated solely off infinite wing data which is more readily available. This method also allows us to examine the circulation distribution of wings with different planform shapes and geometric properties (Anderson, 2016, pp. 465).

The interest of the post stall characteristics translates to aircraft that can intentionally or accidentally experience large angles of attack. One example is fighter planes which are designed to optimize maneuverability by quickly pulling high angles of attack (Anderson 2016, pp. 465). Stunt planes are another application where the post stall characteristics would be of interest to an aerodynamicist. The stunt pilot intentionally climbs rapidly entering the post stall region and as a result enters a helical spin downwards. Three different types of spin can occur after incipient stall. If the pilot does not correct the stall by pushing the nose of the aircraft down to decrease the angle of attack, fully developed spins occur that take three different shapes: erect spin, inverted spin, and flat spin (Houston, S. 2021, pp. 1)

Although stunt pilots intentionally enter spins to please viewers, stall and spin can happen accidentally in any aircraft. Knowing how to regain control of the aircraft in this dangerous situation takes an experienced pilot. With the few examples of flight at stall mentioned above, there are practical reasons to extend Prandtl's classical lifting line to estimate at what angle of attack stall will occur for a finite wing.

2 - Methods

2.1 Classical Lifting Line Theory

The classical lifting line theory presented below is based on the notation used in "Fundamentals of Aerodynamics" (Anderson, 2016, pp. 427-442). For a wing generating lift, the bulk pressure distribution is greater on the bottom than the top. At the wingtips, the

high-pressure region on the bottom must "leak" to the top due to the pressure gradient, introducing a spanwise flow variation that changes the aerodynamic properties. The creation of vortices at the wingtips parallel to the direction of the flow that cause an inward circulation toward the center span can be seen in Figure 1. This induced velocity imparted onto the wing due to the wingtip vortices is called the downwash velocity denoted as w .

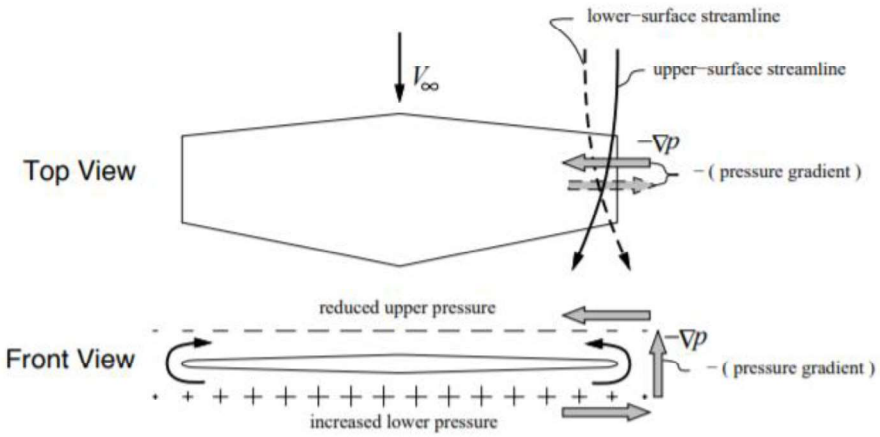

Figure 1: Illustration of Downwash on a Finite Wing

The result of this downwash velocity is that the finite wing experiences an angle of attack less than that of an airfoil called the effective angle of attack α_{eff}. This is caused by the downwash velocity shifting the local relative velocity vector downwards. Physically, the downwash velocity pushes the wing down, decreasing its angle of attack. The second concept that arises due to downwash velocity is the creation of induced drag. Since the local relative velocity vector is shifted at an angle of incidence equal to the induced angle of attack α_i shown in Figure 2, the downwash on a finite wing causes a force vector parallel to the free stream velocity. This force vector is termed the induced drag. The geometric angle of attack α is the angle of attack someone would witness as the wing is tilted. The crutch of Prandtl's classical lifting line theory is the relationship between a finite wing's aerodynamic properties and the airfoils aerodynamic properties:

$$\alpha_{eff} = \alpha - \alpha_i \tag{1}$$

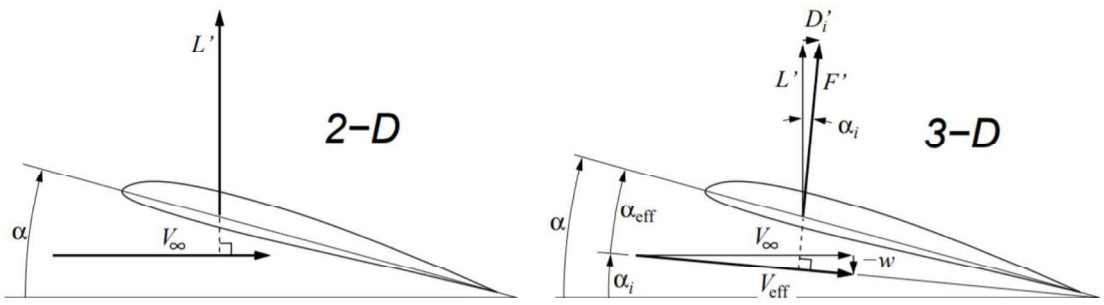

Figure 2: Difference Between Geometric and Aerodynamic Properties of an Airfoil and Finite Wing

With these new geometric properties of a finite wing established and the knowledge of the trailing vortices on each wingtip that creates circulation around the wing, Prandtl originally represented an arbitrary finite wing shown in Figure 3 as a horseshoe vortex. The horseshoe vortex consists of a bound vortex representing the wing, and two free vortices that represent the trailing vortices at the wingtip. The free trailing vortices must continue downstream to satisfy Helmholtz's theorem.

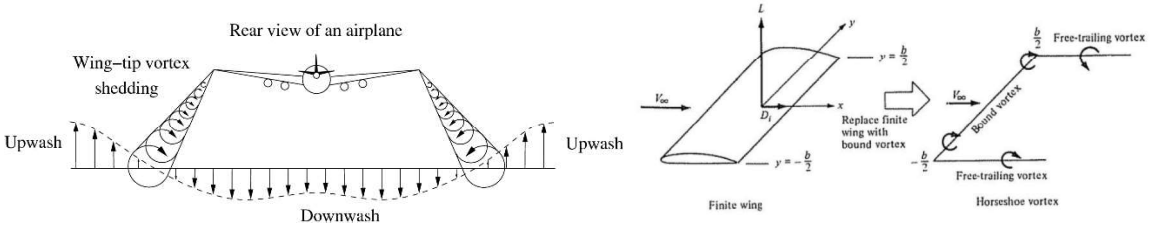

Figure 3: Mathematical Representation of the Finite Wing

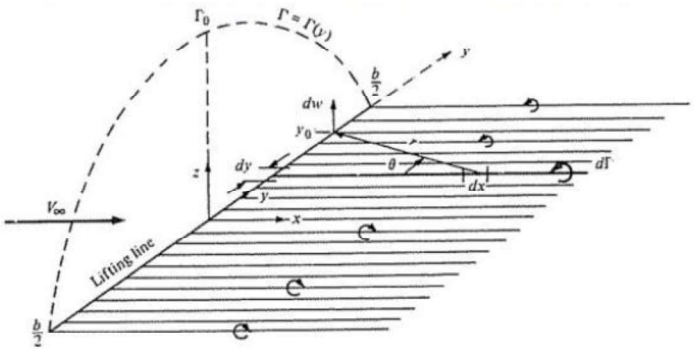

Figure 4: Superposition of an Infinite Number of Horseshoe Vortices Along the Lifting Line

After realizing that the single horseshoe vortex did not accurately simulate that of a finite wing, the model was changed to superimpose an infinite number of small horseshoe

vortices coincident along a line hence called the lifting line shown in Figure 4. The circulation varies along the bound vortices and each horseshoe vortex defines a value of circulation Γ along the lifting line. The infinite number of horseshoe vortices creates a continuous distribution of circulation along the wing. Evaluating an infinitesimally small segment dy of the lifting line at a local span coordinate, the total downwash velocity induced at that coordinate due to all the trailing vortices can be evaluated by:

$$w(y_0) = -\frac{1}{4\pi}\int_{-b/2}^{b/2}\frac{\left(d\Gamma/dy\right)}{(y_0 - y)}dy \tag{2}$$

Using the geometrical relationship in equation (1) the spanwise induced angle of attack in terms of the circulation distribution along the wing can be defined as:

$$\alpha_i(y_0) = \frac{1}{4\pi V_\infty}\int_{-b/2}^{b/2}\frac{\left(d\Gamma/dy\right)}{(y_0 - y)}dy \tag{3}$$

To represent the effective angle of attack based on the circulation distribution, the Kutta-Joukowski theorem is defined based on Figure 4:

$$L' = \frac{1}{2}\rho_\infty V_\infty c(y_0)c_l = \rho_\infty V_\infty \Gamma(y_0) \tag{4}$$

where the chord length $c(y_0)$ varies along the span. If the lift coefficient of an airfoil according to thin airfoil theory is defined as:

$$c_l = a_0\left[\alpha_{eff}(y_0) - \alpha_{L=0}\right] = 2\pi\left[\alpha_{eff}(y_0) - \alpha_{L=0}\right] \tag{5}$$

then equation (4) can be substituted into equation (5) to yield the definition of the effective angle of attack α_{eff} after some rearrangement:

$$\alpha_{eff}(y_0) = \frac{\Gamma(y_0)}{\pi V_\infty c(y_0)} + \alpha_{L=0} \tag{6}$$

Substituting equation (6) into equation (1) we get the fundamental equation of Prandtl's lifting line theory which is a statement that the geometric angle of attack is equal to the sum of the effective angle of attack plus the induced angle of attack; all based on the circulation distribution of the finite wing.

$$\alpha(y_0) = \underbrace{\frac{\Gamma(y_0)}{\pi V_\infty c(y_0)} + \alpha_{L=0}}_{\alpha_{eff}(y_0)} + \underbrace{\frac{1}{4\pi V_\infty}\int_{-b/2}^{b/2} \frac{\left(d\Gamma/dy\right)}{(y_0 - y)} dy}_{\alpha_i(y_0)} \tag{7}$$

A more extensive explanation of Prandtl's lifting line theory can be read in "Fundamentals of Aerodynamics" (Anderson, 2016, pp. 423-464), however for this paper, the numerical implementation of this theory can be sufficiently understood from equation (7).

2.2 Numerical Implementation

The numerical lifting line theory used in this paper was implemented based on Anderson's method presented in "Fundamentals of Aerodynamics" (Anderson, 2016, pp. 465-567). A detailed list of steps with an accompanying program flow chart are provided:

1. Define the geometric and flow properties of the finite wing (span, geometric angle of attack, taper ratio, free stream velocity, etc.) Discretize the wing into k+1 spanwise stations. Create an array of chord lengths at each spanwise station.
2. For the defined wing at a specified geometric angle of attack, assume an initial circulation distribution that includes all the spanwise stations. Assuming an elliptical distribution with Γ_0 as any arbitrary number is sufficient.

$$\Gamma_{input,0} = \Gamma_0 * \sqrt{1 - \left(\frac{2y}{b}\right)^2} \tag{8}$$

3. Calculate the induced angle of attack at each spanwise station given the circulation distribution:

$$\alpha_i(y_n) = \frac{1}{4\pi V_\infty}\int_{-b/2}^{b/2} \frac{\left(d\Gamma/dy\right)}{(y_n - y)} dy. \tag{9}$$

   The derivative is calculated with a first order forward finite difference method. After differentiating, the integral is evaluated using Simpson's rule. The numerical representation of the above integral using Simpson's rule can be found in "Fundamentals of Aerodynamics" along with a brief discussion of numerical singularities.
4. Calculate the effective angle of attack.

$$\alpha_{eff}(y_n) = \alpha - \alpha_i(y_n) \tag{10}$$

5. Using infinite wing data, obtain the spanwise section lift coefficient $(c_l)_n$ at the calculated effective angle of attack α_{eff}. Linear interpolation can be used to approximate the airfoil lift coefficient.
6. Calculate a new reference circulation using the Kutta-Joukowski theorem:

$$\Gamma(y_n) = \frac{1}{2} V_\infty c_n (c_l)_n \tag{11}$$

where c_n is the local chord section.

7. Compare the input circulation to the new value of circulation at each spanwise section. If the two do not agree within a specified tolerance (0.005 is reasonable), update the input circulation determined by:

$$\Gamma_{input} = \Gamma_{input} + D\left(\Gamma_{new} - \Gamma_{input}\right) \tag{12}$$

where D is the damping factor which determines the severity of the update for convergence (usually around the value of 0.05).

8. Repeat these steps until the input circulation is reasonably close to the new value of circulation.
9. With the converged circulation distribution, the aerodynamic properties for the finite wing can then be calculated.

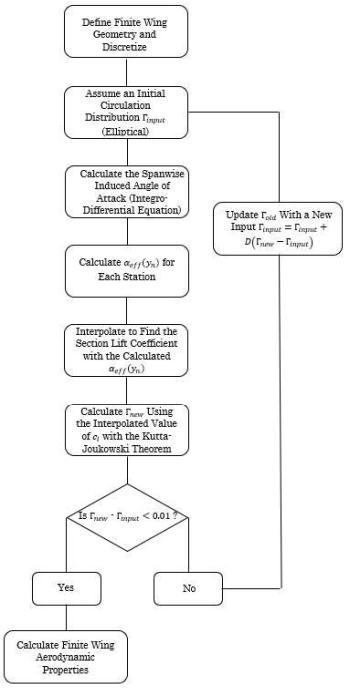

Figure 5: Flow Chart of Numerical Implementation

3 - Code Development and Testing

3.1 NACA 0015 Wing

The numerical lifting line code shown in Appendix A was written in MATLAB®. To verify the validity of the code presented in this paper, the results were compared to Anderson's implementation for a NACA 0015 wing for geometric angles of attack ranging from zero to fifty degrees. The section lift data shown as the dashed blue line was taken from infinite wing data collected at the University of Maryland (Saini, 1979, pp. 46). The experimental wing data came from the same source. The wing characteristics used as inputs to the code are shown in Table 1 and are based on the geometry of the NACA 0015 experimental wing (Saini, 1979, pp. 46). The velocity was calculated based on the Reynolds number and the experimental wings chord length.

Table 1: NACA 0015 Inputs for Code Validation

Airfoil Section	NACA 0015
Span (b)	0.3515 [m]
Chord Length (c)	0.127 [m]
Aspect Ratio (AR)	2.768
Taper Ratio (λ)	1 (Rectangular)
Reynolds Number (Re)	350,000
Free Stream Velocity (V_∞)	39.1531 [m/s]

Since the program linearly interpolates the lift coefficient based on the estimated effective angle of attack, if the curve starts at 0 degrees, some data for negative angles of attacks must be provided. Since the lift curve is linear at low angles of attack and data was not provided for any negative angles of attack, it was reasonable to mirror the positive lift coefficient values for the first 2 degrees as negative so a complete curve could be created.

The present numerical results are shown in Figure 6. The input section lift coefficients, finite wing experimental data, lift coefficient curve from classical lifting line theory and Anderson's numerical solution are also shown (Anderson, 1980, pp. 901). The numerical implementation calculates the lift coefficients for the linear pre-stall region better than the classical linear lifting line theory. From the graph, the present code

matches Anderson's numerical results within close agreement. Anderson's code predicts the maximum stall at the critical angle of attack with more accuracy, however the present code seems to be more accurate over the entire spread of data shown in Figure 7. This may be due to the different aspect ratios used since the present code has an aspect ratio based on the experimental finite wing's geometry. The numerical results show large inaccuracies around 40 degrees and at incipient stall which is approximately 17 degrees. For this airfoil section, the numerical code predicts the lift coefficient of stall within 0.53% which shows the accuracy of this method for this wing.

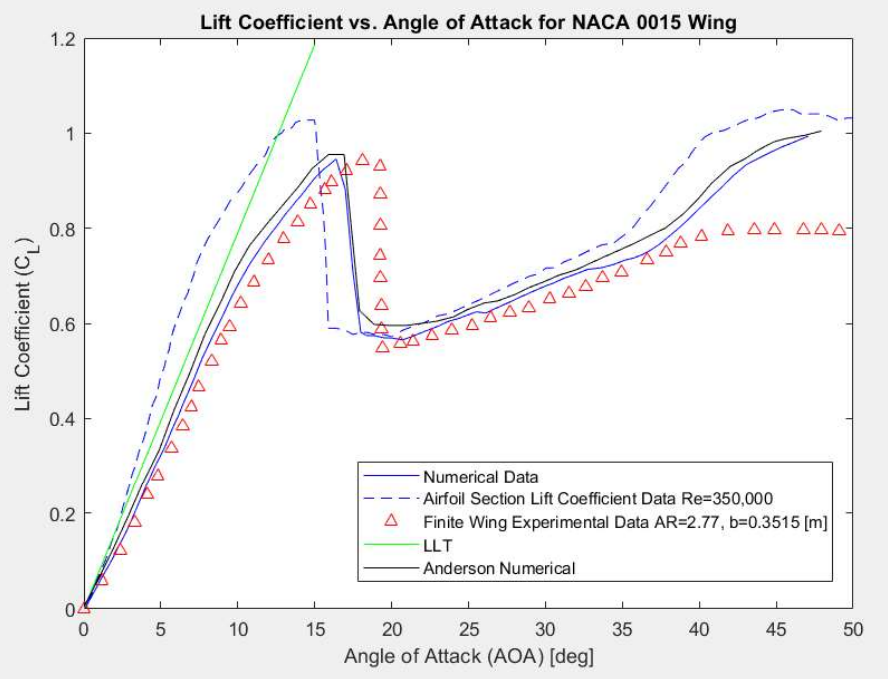

Figure 6: Numerical Lifting Line Results

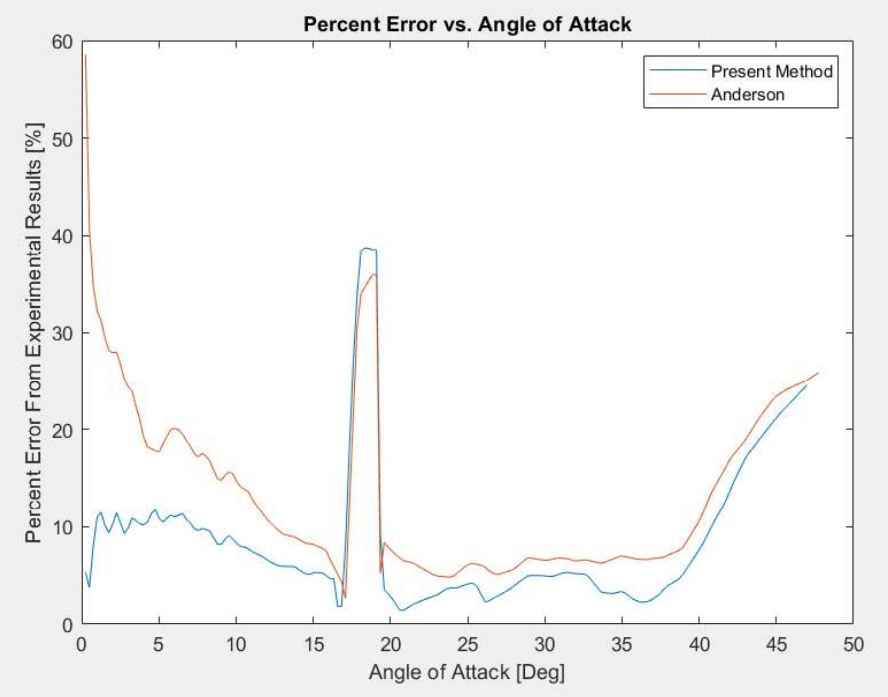

Figure 7: Percent Error of Numerical Lifting Line Code

The code converges well for a rectangular and tapered wing with a NACA 0015 cross section. Figure 8 shows the circulation distribution for each iteration of a rectangular wing with an aspect ratio of 2.77 and a span of 0.3515 m. The distribution starts out elliptical and converges to a shape more representative of a rectangle. This indicates that the program can distinguish the geometrical properties input by the user.

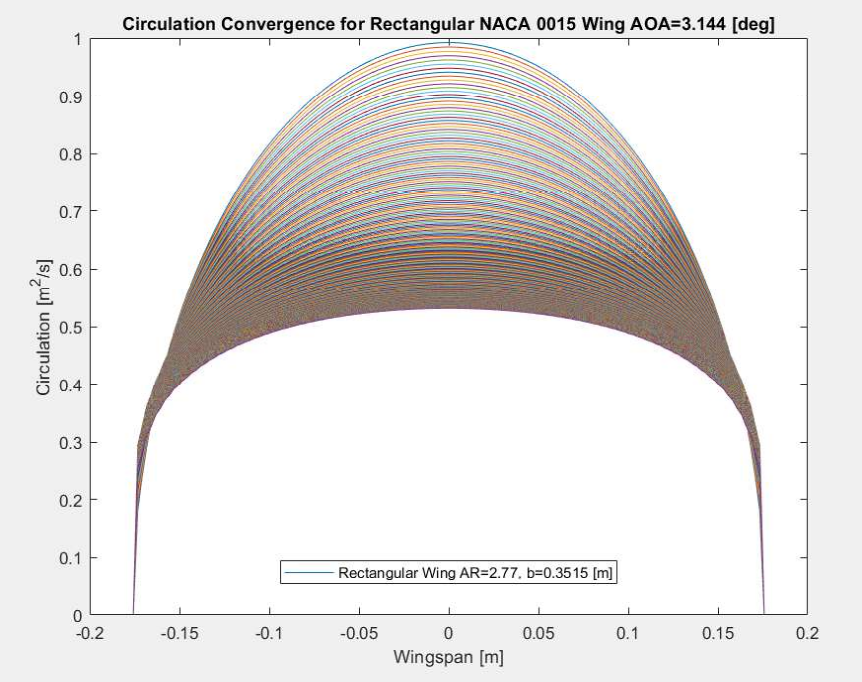

Figure 8: Circulation Convergence of a NACA 0015 Rectangular Wing AOA=3.144 deg

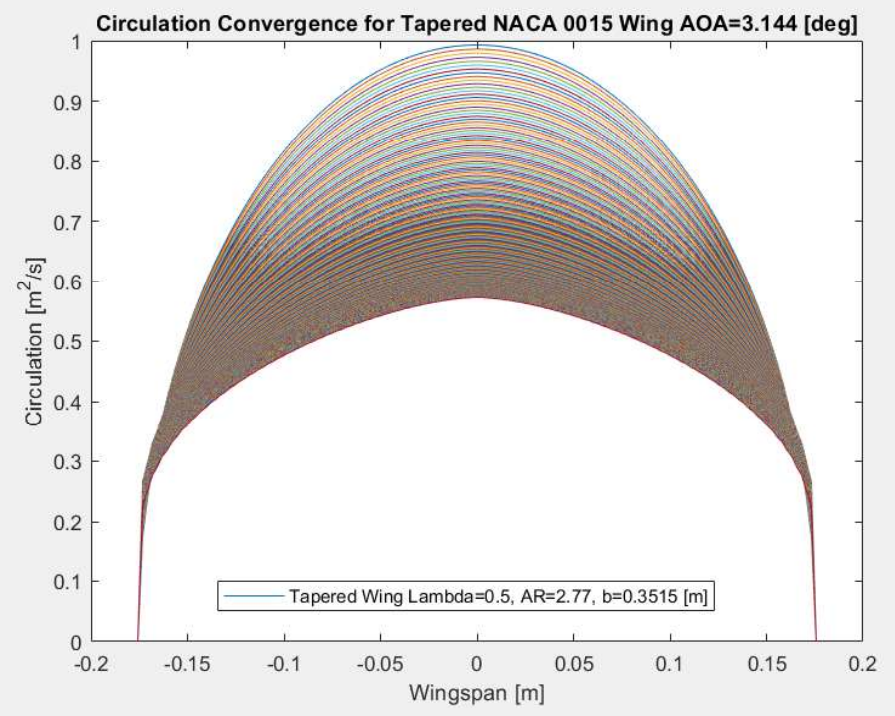

Figure 9: Circulation Convergence of a NACA 0015 Tapered Wing AOA=3.144 deg

Figure 9 shows the circulation convergence for a tapered wing with a taper ratio of 0.5, aspect ratio of 2.77 and a span of 0.3515 m. Just like the rectangular wing, the solution

starts out with an elliptical lift distribution and converges to a triangular shape representative of the tapered wing. Figure 9 also shows the ability of the code to recognize the properties of a tapered wing.

A plot of both converged circulation distributions for the rectangular wing and the tapered wing are shown in Figure 10. Both wings have the same mean chord. The circulation for the tapered wing reaches a higher maximum than the rectangular wing and the taper decreases the magnitude of circulation near the wingtips.

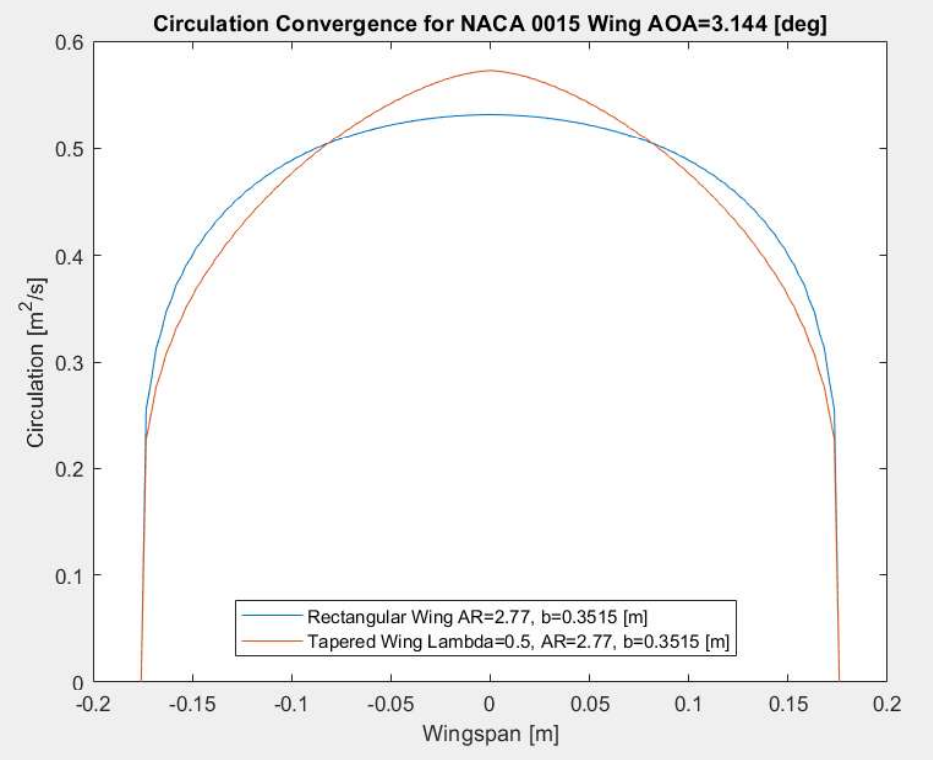

Figure 10: Circulation Convergence of a NACA 0015 Rectangular and Tapered Wing AOA=3.144 deg

Figures 11,12, and 13 show the circulation convergence of the wing at one of the nonlinear regions of the lift coefficient curve. The shapes are still representative of the wing shapes however, they show a much more complex circulation distribution along the wing.

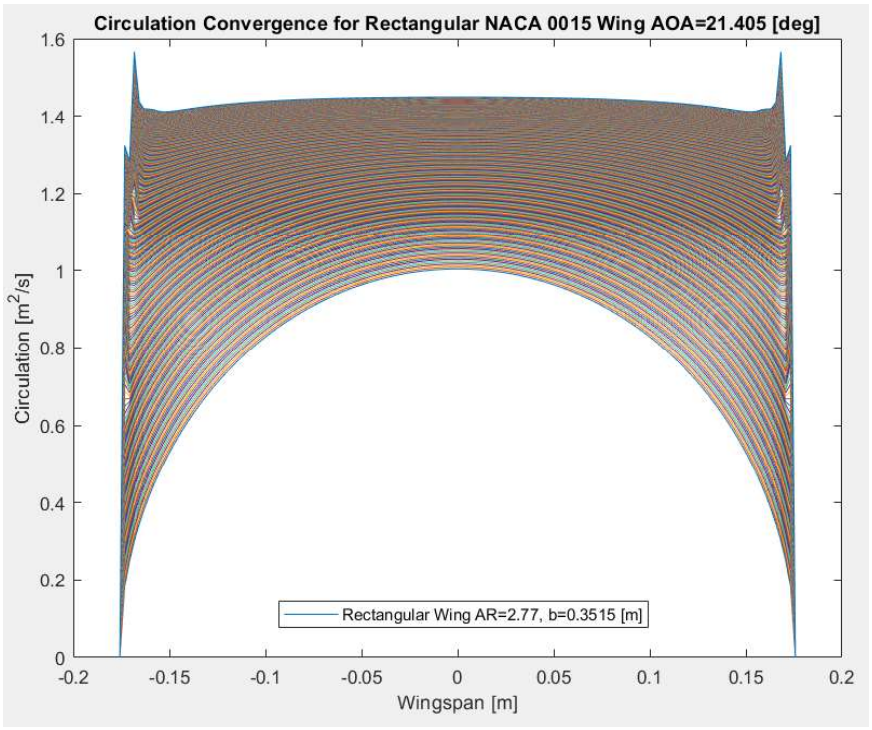

Figure 11: Circulation Convergence of a NACA 0015 Rectangular Wing AOA=21.405

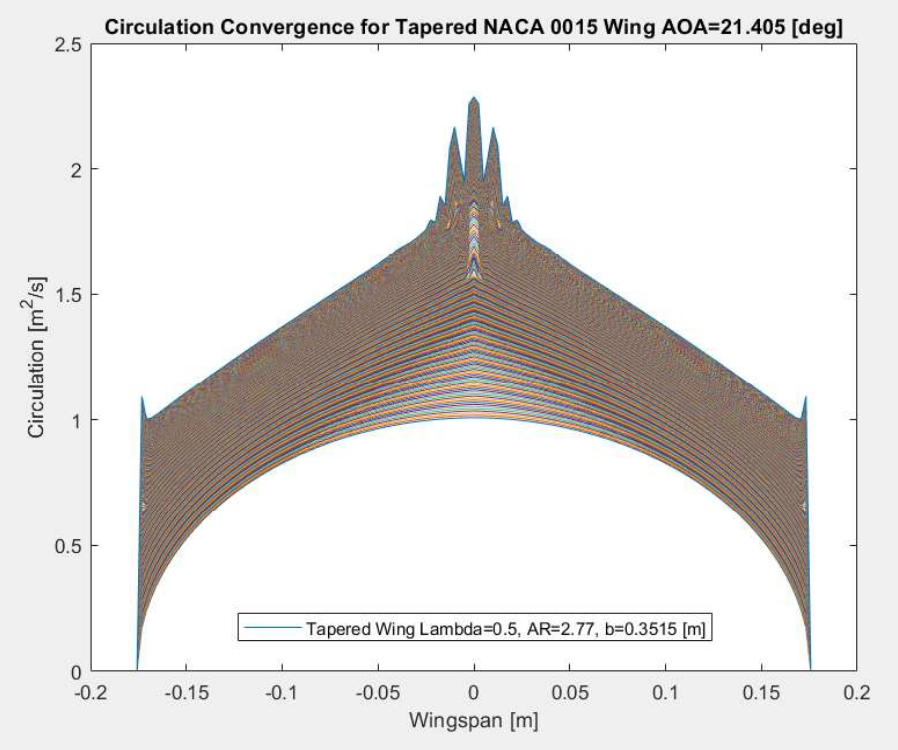

Figure 12: Circulation Convergence of a NACA 0015 Tapered Wing AOA=21.405

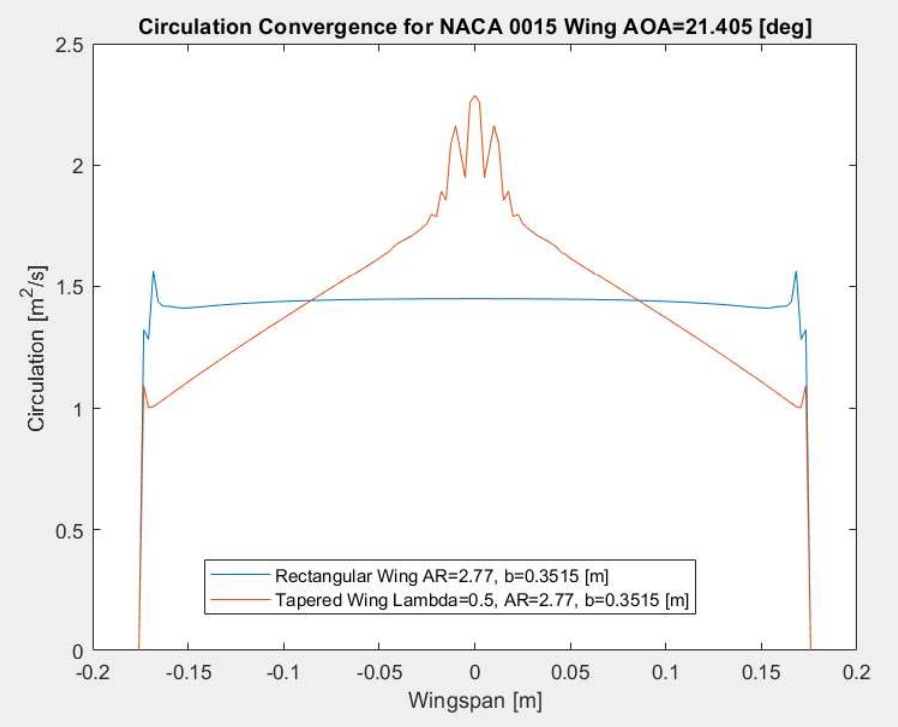

Figure 13: Circulation Convergence of a NACA 0015 Rectangular and Tapered Wing AOA=21.405

3.2 NACA 4418 Wing

The same code used for the NACA 0015 wing was applied to airfoil and wing data for a NACA 4418 section (Ostowari et. al, 1956, pp. 21-27). The properties of the finite wing used in the experimental procedure is shown in Table 2. In the experiments by Ostowari et. al, the experimental wing aspect ratio is 4.5 since a reflection plane model was used (Ostowari et. al, 1956, pp. 2). A summary of scale models used for wind tunnel testing, including reflection plane models can be read in Muncey et. al.

Table 2: NACA 4418 Inputs for Code Validation

Airfoil Section	NACA 4418
Span (b)	2.745 [m]
Chord Length (c)	0.610 [m]
Aspect Ratio (AR)	4.5 (Half Model)
Taper Ratio (λ)	1 (Rectangular)

Reynolds Number (Re)	250,000
Free Stream Velocity (V_∞)	5.8225 [m/s]

The numerical and experimental results are shown in figure 14. For this cambered airfoil with 4% camber 40% along the chord, the numerical lifting line code also predicts the experimental lift coefficient curve reasonably well. The accuracy is not as great as the NACA 0015 wing and the maximum lift coefficient at stall is overestimated by 5.38%. A lot of the data is within 10% error with some points having much greater accuracy as shown in figure 15. The numerical results for the post stall region of this cambered airfoil shows large inaccuracies at 35 degrees. This highlights some of the limitations behind this numerical implementation. At high angles of attack, the flow is highly three dimensional with unsteady flow effects. This numerical implementation is a crude approximation of the three-dimensional flow effects at large angles of attack. At low angles of attack, lifting line theory provides reasonable accuracy with its assumptions.

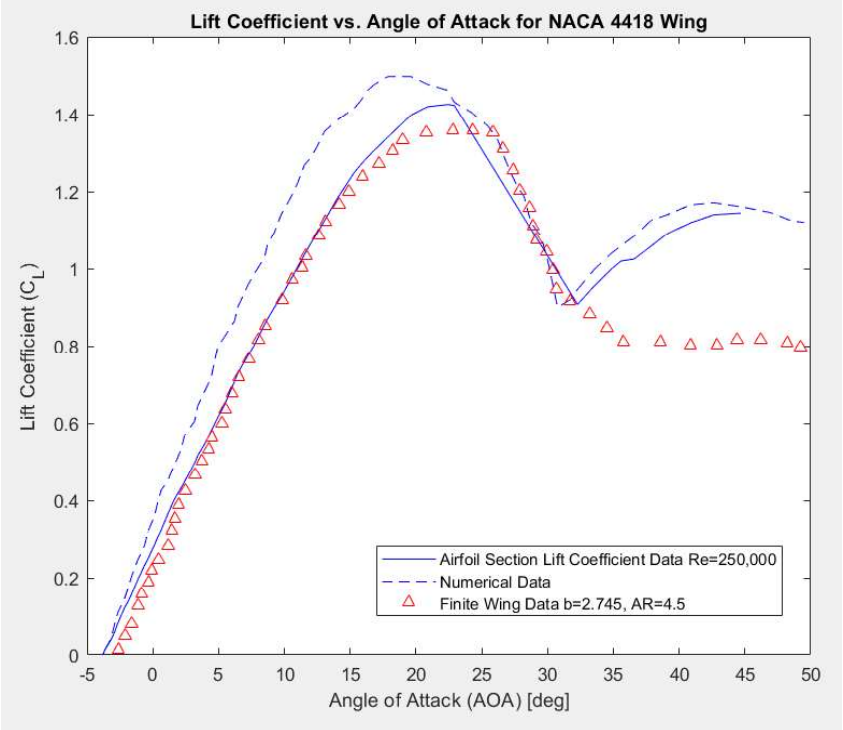

Figure 14: Lift Coefficient Curve for a NACA 4418 Wing with AR=4.5, b=2.745

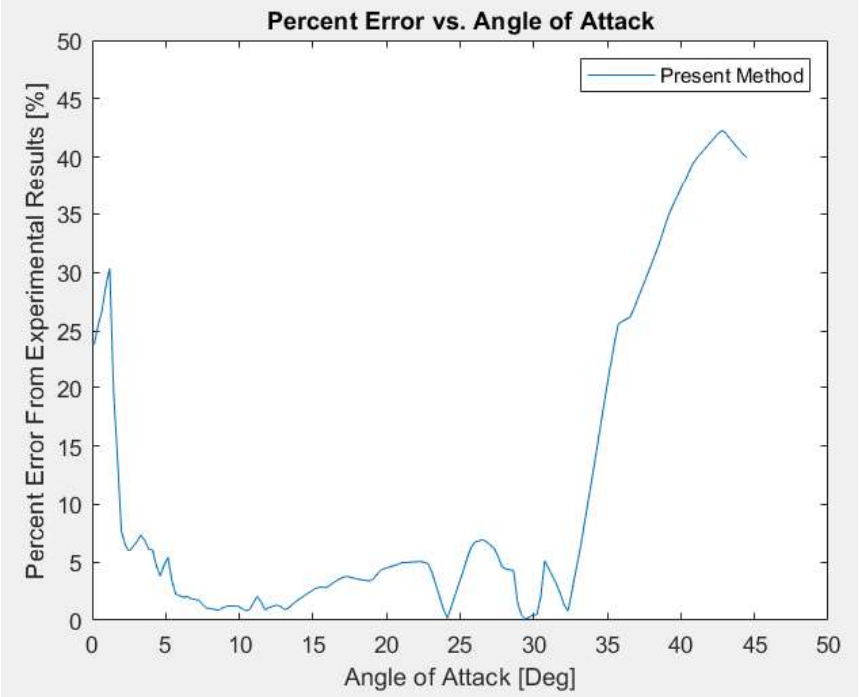

Figure 15: Lift Coefficient Curve for a NACA 4418 Wing with AR=4.5, b=2.745

4 - Discussion

The numerical lifting line presented above shows the ability to obtain reasonably accurate results for prediction of lift coefficients in both the linear and post stall regions with little computational expense. Since the numerical method relies on section lift coefficient data, it is important that accurate data is used. The analysis of a NACA 0015 wing showed the ability of the program to recognize geometry inputs and provide reasonable results. Caution should be used with this method when using some low aspect ratio wings and when data greater than 40 degrees is of interest because they are typically dominated by three-dimensional, unsteady flow effects which are not approximated in lifting line theory.

With reasonable results for validating the model, the numerical lifting line code based on the NACA 0015 and NACA 4418 models were implemented to see varying effects of three different parameters on the performance of a rectangular wing in the post stall region.

4.1 Effects of Camber

Adding camber to an airfoil changes the performance in many ways compared to a symmetrical airfoil. The distinguishable aerodynamic feature for a cambered airfoil is that the zero-lift angle of attack $\alpha_{L=0}$ is below 0 degrees whereas the zero-lift angle of attack for a symmetrical airfoil is 0 degrees. This allows the cambered airfoil to provide more lift at the same angle of attack. The lift coefficient curves for the NACA 0015 and NACA 4418 wing using the numerical lifting line code and the same wing properties is shown in figure 16. Adding camber translates the entire curve upwards with the maximum lift at stall approximately 55% higher than the NACA 0015 wing. There is also a less precipitous drop in lift for the cambered airfoil at stall than the symmetrical wing.

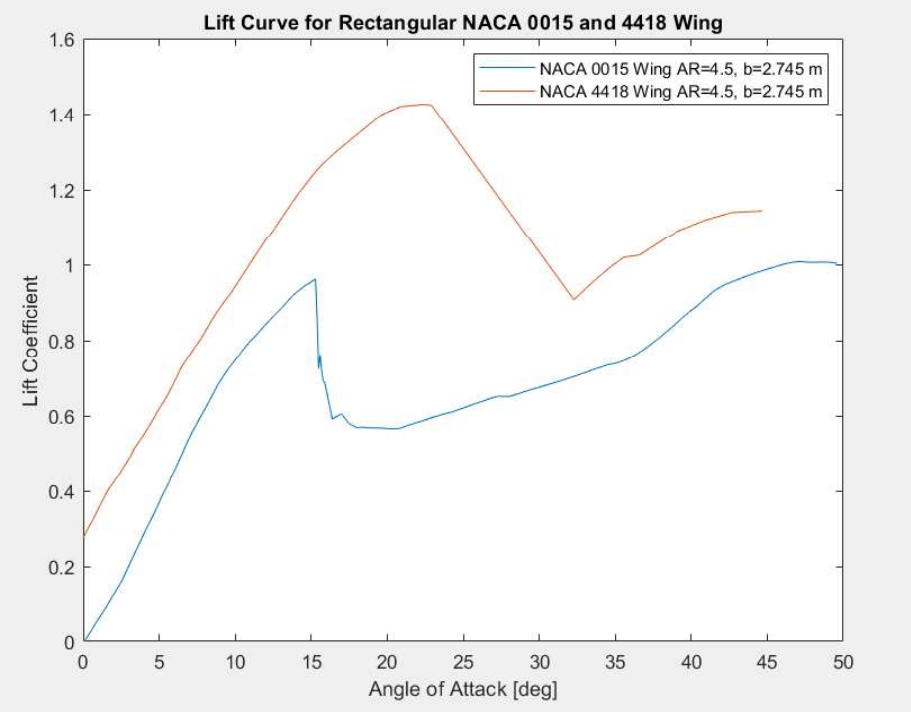

Figure 16: Lift Coefficient Curve for a NACA 4418 and NACA 0015 Wing with AR=4.5, b=2.745

4.2 Effects of Reynolds Number

Using section lift data for a NACA 4418 airfoil at Reynolds numbers of 0.25e6 and 1e6, the numerical lifting line code was used to estimate the lift coefficients for a finite wing with the same dimensions. At higher Reynolds numbers, the maximum lift coefficient decreases. For this wing, there seems to be a small dependency on Reynolds number for the

post stall region after 35 degrees. At these high angles of attack, the wing's flow characteristics are dominated by turbulence and wake drag anyway such that increasing the Reynolds number has little effect on the lift coefficients beyond a certain point.

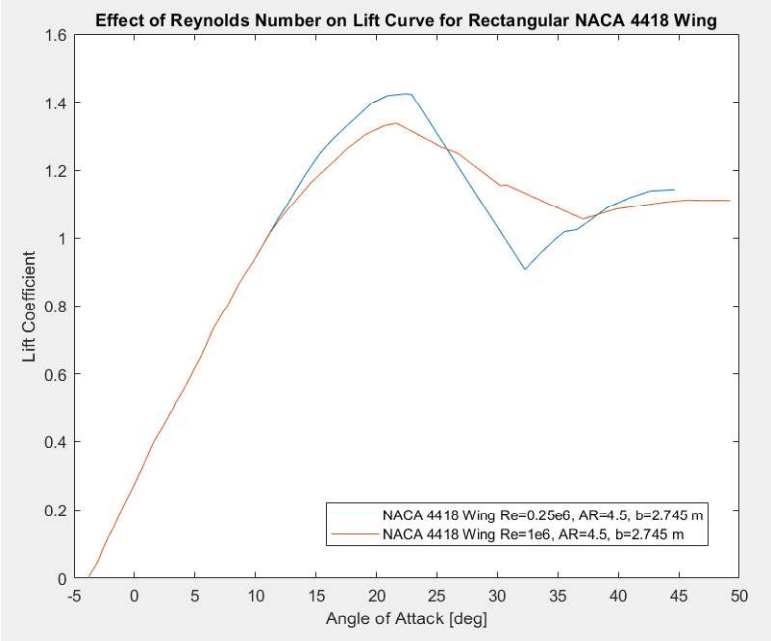

Figure 17: Lift Coefficient Curve for NACA 4418 Wing of AR=4.5, b=2.745 and Varying Reynolds Number

4.3 Effects of Aspect Ratio

The numerical lifting line code was used to plot the lift coefficients for a NACA 4418 wing with aspect ratios of 4.5, 12, and 20 shown in Figure 18. There is no significant effect of aspect ratio on the post stall characteristics for larger ratios predicted by the numerical lifting line theory. For smaller aspect ratios, the nonlinear region is translated downward but the effects are more significant in the linear region. The maximum lift coefficient and lift curve slope decreases with decreasing aspect ratio. The physical interpretation gained from the spanwise circulation distributions shown in figure 19 is that wings of small aspect ratios have much more downwash. Practicality in mind the larger the aspect ratio, the more difficult it is for the aircraft to maneuver. This may increase difficulty to pull out of a stall induced spin and gives insight into one of the reasons why fighter jets and stunt planes have small aspect ratios.

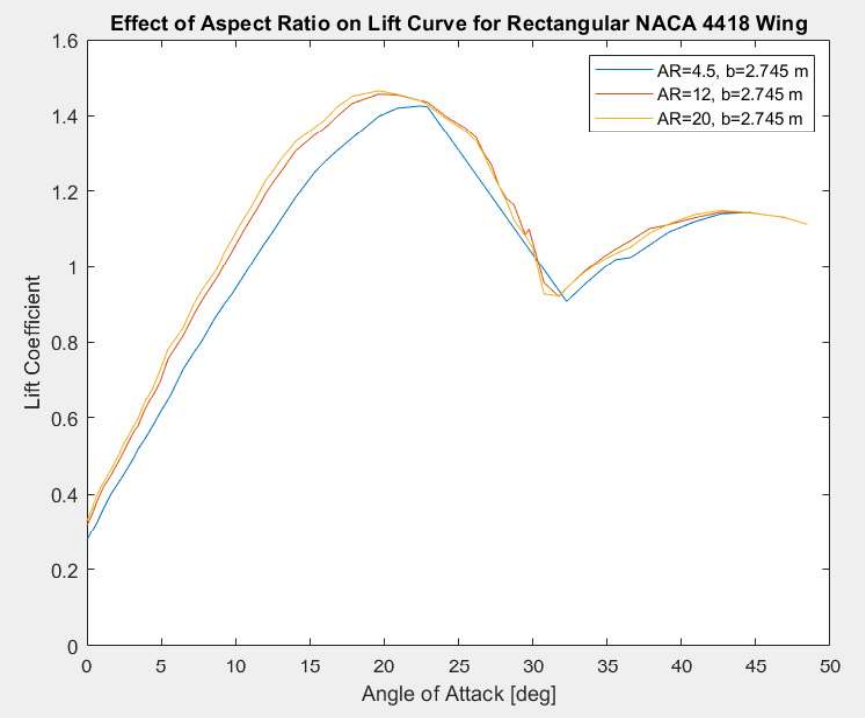

Figure 18: Effect of Aspect Ratio on Lift Coefficient Curve NACA 4418 Wing

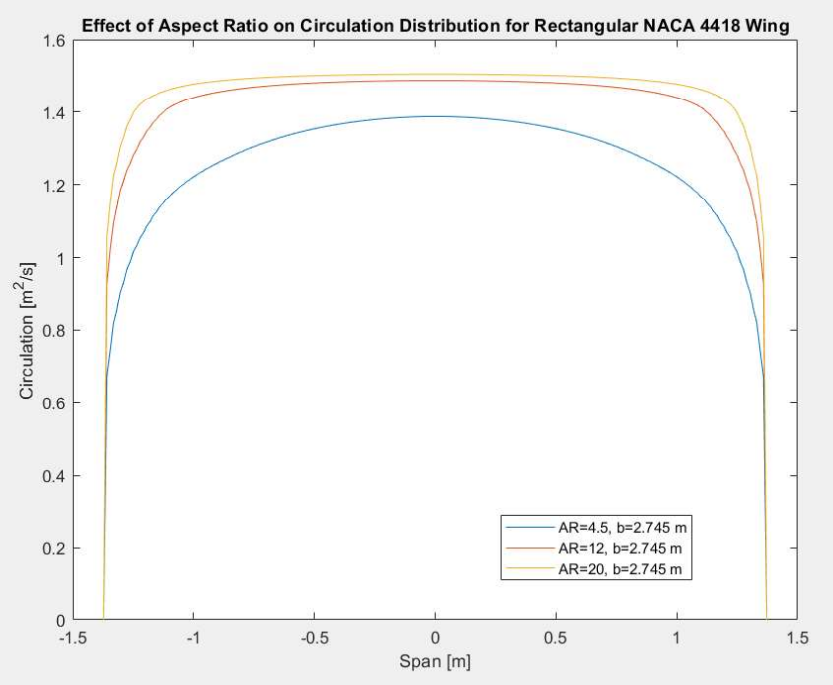

Figure 19: NACA 4418 Rectangular Wing Circulation Distribution for Different Aspect Ratios

Figure 20 shows the effect of aspect ratio on induced drag coefficients. As the aspect ratio increases, the induced drag decreases. This is because the effect of downwash is less significant for larger aspect ratio wings.

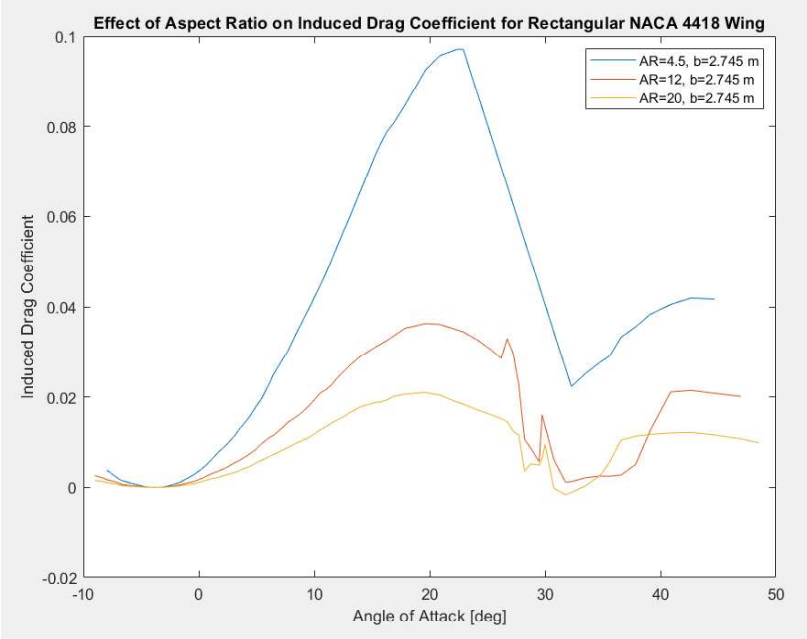

Figure 20: Effect of Aspect Ratio on Induced Drag for a NACA 4418 Wing

5 - Conclusions

Using the nonlinear lifting line theory presented by Anderson, reasonable results for aerodynamic properties of lift and drag coefficients for a NACA 0015 and 4418 wing were achieved. For both airfoil sections, accuracy of about 10% or less was obtained for more than half of the data with much higher accuracy in certain regions. The numerical implementation was able to calculate the maximum lift at stall well with an underestimation of the critical angle of attack. The use of this method could inform an airplane designer the angle of attack to expect stall and thus know how to avoid it. This method generally works for different straight wing shapes and geometric properties with moderate to high aspect ratios. The numerical solution can be done with minimal computational expense which makes this method a very practical way to investigate preliminary wing properties. The numerical lifting line also predicts linear regions of the lift curve better than the classical lifting line theory which is practical as well. It is also important to recognize the limitations of this method. Low aspect ratio wings, swept wings and delta wings are highly governed by three-dimensional flow. In addition, the post stall

region is also governed by three-dimensional unsteady flow effects which is why the error in the above models increase dramatically at around 40 degrees angle of attack. Depending on the application, alternative methods may yield better results.

6 - Future Work

If given the opportunity to continue with this numerical lifting line code, I would like to elaborate on the effect of taper ratio. The effect of some other properties of a straight wing such as wash in, washout and variable airfoil sections of the wing would be interesting to investigate as well.

If given the opportunity to choose another research topic in aerodynamics, I would like to investigate the aerodynamic properties of swept wings with low aspect ratios. These are wings typically used for high maneuverability fighter jets. This could be achieved using the vortex lattice numerical method. An interesting adaptation of the vortex lattice method would be the introduction of compressibility effects if possible. This would allow for further investigation of the wing operating at higher velocities where compressibility effects cannot be neglected.

References

Anderson. (2016). *Fundamentals of aerodynamics* (6th ed.). McGraw-Hill Education.

Anderson, J. D., Corda, S., & Van Wie, D. M. (1980). Numerical lifting line theory applied to drooped leading-edge wings below and above stall. *Journal of Aircraft, 17*(12), 898-904. doi:10.2514/3.44690

Houston, S. (2021, February 07). Aircraft spins 101. Retrieved May 12, 2021, from https://blog.globalair.com/post/2014/05/30/Aircraft-Spins-101#:~:text=Erect%20Spin%3A%20Erect%20spins%20are,roll%20occurs%20in%20opposite%20directions.

Kaushik M. (2019) Finite Wing Theory. In: Theoretical and Experimental Aerodynamics. Springer, Singapore. https://doi.org/10.1007/978-981-13-1678-4_6

Koyama, K., & Koyama, K. (2013). Relation between the lifting surface theory and the lifting line theory in the design of an optimum screw propeller. *Journal of Marine Science and Technology, 18*(2), 145-165. doi:10.1007/s00773-012-0200-3

Drela, M. Introduction to 3-D wings. MITOPENCOURSEWARE

Muncey, J. J., & Pote, D. M. (1956). *REPORT 20 o - h- a: O o_ ADVISORY GROUP FOR AERONAUTICAL DESIGN AND CONSTRUCTION OF WIND TUNNEL MODELS*

Ostowari, C., & Naik, D. (1985). *Post-stall wind tunnel data for NACA 44XX series airfoil sections A subcontract report*

Saini, J. K. (1979). *An Experimental Investigation of the Effects of Leading Edge Modifications on the Post-Stall Characteristics of an NACA 0015 Wing* (Unpublished master's thesis). UMCP Severn Library University Archives - Theses & Dissertations.

Appendix A: Numerical Lifting Line Code

```
% Program Written by Andrew Simin
% This program implements a numerical lifting line theory for prediction of
% post stall aerodynamic coefficients.
% All underlines are parameters to be input by the user
% Flow properties is a section for comparison to experimental data, otherwise the
% only input needs to be velocity
% Program outputs lift and induced drag for a finite wing

clear all
close all
clc

%% Load section lift data

data = load('_____');                                   % load section lift
data
AOA_2D = data(1:end,1)';                                % experimental angle
of attack
cl_2D = data(1:end,2)';                                 % experimental lift
coefficient
[AOA_2D unique_indices] = unique(AOA_2D)                % return unique
indices for interpolation
cl_2D = cl_2D(unique_indices)                           % return unique
values of cl
clear unique_indices
%% Input data

k = 140;                                                % number of stations
noi = 400;                                              % number of
circulation update iterations
damping_factor = 0.01;                                  % damping factor

%% Define wing properties
b = ______;                                             % wing span
lambda = _____;                                         % taper ratio
AR = ______;                                            % aspect ratio
% planform area
s = (b^2)/AR;                                           % planform area
rc = 2*s/(b*(1+lambda));                                % root chord
tc = rc*lambda;                                         % tip chord

%% Flow properties
Re_test = ______                                        % test reynolds
number (optional)
nu_inf = 1.4207E-5                                      % kinematic viscosity
[m^2/s]
char_chord_length = ______                              % chord length [m]
(optional)
% V_inf = 39.1531                                       % free stream
velocity [m/s]
V_inf = (Re_test*nu_inf)/c                              % velocity based on
experimental reynolds # [m/s]

%% Loop through geometric angles of attack based on input data
for a = 1:length(AOA_2D)

AOAd_geo = AOA_2D(1,a);                                 % geometric angle of
attack [deg]
AOAr_geo = deg2rad(AOAd_geo);                           % geometric angle of
attack [rad]

%% Anderson numerical implementation

%% 1) Discretize wing
y = 0:k;                                                % number of y
coordinates (k+1)
dy = b/k;                                               % distance between
spanwise coordinates
y = y'*dy - b/2;                                        % y coordinates
```

```
chord = ((2*s)/((1+lambda)*b))*((1-((1-lambda)/b)*2*abs(y)))                % chord length along
span
%chord = sqrt(1-(2*y/(b)).^2)
%% 2. Asuume elliptical lift distribution
gamma = 1 * sqrt(1-(2*y/b).^2);                                             % assume elliptical
distribution

% allocate storage
dgamma_dy = zeros(k+1,1);                                                   % allocate storage
for dgamma_dy
I = zeros(k+1,1);                                                           % allocate storage
for integral
f = zeros(k+1);                                                             % allocate storage
for function inside integral
Error = zeros(noi,1);                                                       % allocate storage
for error between new gamma and old gamma

for i = 1:noi
%% 3. Compute induced angle of attack

for t = 1:k/2
    dgamma_dy(t) = (gamma(t+1) - gamma(t)) / dy;                            % calculate dgamma_dy
for negative y values
end

dgamma_dy(k/2+1) = 0;                                                       % define gamma = 0 at
center span

for t = k/2+2 : k+1
    dgamma_dy(t) = (gamma(t) - gamma(t-1)) / dy;                            % calculate dgamma_dy
for positive y values
end

% Calculation of the integral
    for n=1:k+1
        for j=1:k+1
            if j == n
                f(n,j) = 0;                                                 % average value
between j+1 and j-1 when n = j
            else
                f(n,j) = dgamma_dy(j)/(y(n)-y(j));                          % integrand
            end
        end
        %I(n) = trapz(y,f(n,:));                                            % numerically
integrate
        I(n) = simpsons(f(n,:),y(1,1),y(end,1),[]);
    end

 AOAiR = I ./ (4*pi*V_inf);                                                 % induced AOA [rad]

 %% 4. Commpute alpha effective
 AOAEff = AOAd_geo*pi/180 - AOAiR;


 %% 5. Compute cl
 %cl = 2*pi*(alphaEff - alpha0liftRad); For linear lifting line
 cl = interp1(AOA_2D,cl_2D,rad2deg(AOAEff));                                % interpolate section
cl with effects of downwash
 %% 6. New lift distribution
 gammaNew = 1/2 * V_inf .* chord .* cl;                                     % kutta joukowski
circulation
 gammaNew(1) = 0;                                                           % set circulation at
tip to 0
 gammaNew(end) = 0;                                                         % set circulation at
tip to 0

 if abs(gammaNew - gamma) < 0.01
     break
 end

 %% 7. Gamma update
```

```
 gamma = gamma + damping_factor*(gammaNew - gamma);                          % update circulation
 end

%% 10. Last computations
CL = 2 / ((V_inf)*s) * trapz(y,gamma);                                       % finite wing lift
coefficient
CDi = 2 / ((V_inf)*s) * trapz(y,gamma.*AOAiR);                               % induced drag

%% Plots

plot(AOAd_geo,CL,'^')                                                        % plot individual
data point
hold on

end
hold off

h = findobj(gca,'Type','line')                                               % return graphics
root object
AOA_NLLLT = cell2mat(get(h,'Xdata'))                                         % retrive x data
points
CL_NLLLT = cell2mat(get(h,'Ydata'))                                          % retrieve y data
points
plot(AOA_NLLLT,CL_NLLLT,'-b')

hold on

plot(AOA_2D,cl_2D,'--b')                                                     % plot input data
(section lift coefficients)

data1 = load('0015EXP_Anderson.txt');
xEXP = data1(:,1);
yEXP = data1(:,2);
plot(xEXP,yEXP,'^r')                                                         % plot finite wing
experimental data

data2 = load('0015LLT.txt')
AOA_LLT = data2(1:end,1)
CL_LLT = data2(1:end,2)
plot(AOA_LLT,CL_LLT,'g')                                                     % plot LLT
approximation

ylabel('Lift Coefficient (C_L)')
xlabel('Angle of Attack (AOA) [deg]')
title('Lift Coefficient vs. Angle of Attack for NACA 0015 Wing')

data3 = load('Anderson_Numerical.txt')
xAnd = data3(1:end,1)
yAnd = data3(1:end,2)
plot(xAnd,yAnd,'k')                                                          % plot Andersons
numerical data for comparison
legend('Numerical Data','Airfoil Section Lift Coefficient Data Re=350,000','Finite Wing
Experimental Data AR=2.77, b=0.3515 [m]','LLT','Anderson Numerical')
axis([0 50 0 1.2])

[xEXP unique_indices] = unique(xEXP)                                         % return unique
indices for interpolation
yEXP = yEXP(unique_indices)                                                  % return unique
values of cl
clear unique_indices

[xAnd unique_indices] = unique(xAnd)                                         % return unique
indices for interpolation
yAnd = yAnd(unique_indices)                                                  % return unique
values of cl
clear unique_indices

alpha = linspace(0,50,200)                                                   % alpha for
interpolation
for i = 1:200
```

```
    CL_exp(i) = interp1(xEXP,yEXP,alpha(i));                                % interpolate lift
coefficient
    CL_num(i) = interp1(AOA_NLLLT,CL_NLLLT,alpha(i));                       % interpolate
numerical data
    CL_And(i) = interp1(xAnd,yAnd,alpha(i))                                 % interpolate
Anderson
    perror(i) = abs((CL_exp(i)-CL_num(i))/CL_exp(i))*100                    % percent error
present code
    perrorAnd(i) = abs((CL_exp(i)-CL_And(i))/CL_exp(i))*100                 % percent error
Anderson
end

figure
plot(alpha,perror,alpha,perrorAnd)
title('Percent Error vs. Angle of Attack')
xlabel('Angle of Attack [Deg]')
ylabel('Percent Error From Experimental Results [%]')
legend('Present Method','Anderson')
```